P-22

IN-07

NASA Technical Memorandum 107040

Rapid Calibration of Seven-Hole Probes

A.L. Ericksen, R.W. Gallington, and B.M. Rao
Science Applications International Corporation
San Diego, California

W.S. Barankiewicz
Lewis Research Center
Cleveland, Ohio

September 1995

National Aeronautics and
Space Administration

List of Figures

Figure 1a and b. Seven-Hole Probes: a) Front View Showing Port Numbering Convention and Principle Axes; b) Side View 1
Figure 2. Reference System Definition from Gerner et al. (1984) 4
Figure 3. Angular Region Definitions from Gerner et al. (1984) 4
Figure 4. Probe Calibration Computer Program Flow Chart 7
Figure 5. Reduced Calibration Matrix for Typical Outer Sector 1 8
Figure 6. Functional Flow Chart of Flow Property Subroutines 13
Figure 7. Potential Error Sources in Data Acquisition 14
Figure 8. High Frequency Components of 20 and 40 Hz 16

List of Tables

Table 1. Probe 1 Standard Error Results for the Complete Matrix 10
Table 2. Comparison of Probe 1 Sector 1 Standard Error Results for the Complete Matrix and a Reduced Matrix 10
Table 3. Probe 2 Standard Error Results for Reduced Matrix 1 11
Table 4. Probe 2 Standard Error Results for Reduced Matrix 2 11
Table 5. Probe 2 Standard Error Results for Reduced Matrix 2 Data Using Reduced Matrix 1 Model 12

List of Symbols

A_j = set of four flow properties: α_T, β_T, Co, Cq for low angles and θ, ϕ, Co_n, Cq_n for high angles
C_M = compressibility effect coefficient
Co = total pressure coefficient
Cq = approximate dynamic pressure coefficient
$C_{\alpha a}$ = intermediate angle coefficient
$C_{\alpha b}$ = intermediate angle coefficient
$C_{\alpha c}$ = intermediate angle coefficient
$C_{\alpha T}$ = angle of attack coefficient: low angles
$C_{\beta T}$ = angle of sideslip coefficient: low angles
C_θ = pitch angle coefficient: high angles
C_ϕ = roll angle coefficient: high angles
f_s = sampling frequency
f_c = cutoff frequency
K_{ji} = calibration constant
M = Mach number, or number of constants in regression
N = total number of data points in a given sector
P = probe port pressure
P_o = total pressure
P_∞ = static pressure
t_a = data averaging time
t_s = time between samples
t_e = period of error signal
V = velocity
α = angle of attack
α_T = angle of attack, tangential reference system
β = angle of sideslip
β_T = angle of sideslip, tangential reference system
θ = pitch angle, polar reference system
ϕ = roll angle, polar reference system
σ = standard error

Subscripts
i = number of terms in series expansion
L = local property at probe tip
n = port or sector number (1-7)

1. Introduction/Background

Non-nulling seven-hole probes make simultaneous measurements of flow direction, static pressures and total pressures over wide ranges of flow angles, extending to over 70 degrees off the probe axis. Seven-hole probes can be made very small (2.8 mm outer diameter) to minimize flow disturbances. They have six ports evenly spaced around the probe periphery with one port in the center, as illustrated in Figure 1 taken from Gerner et al. (1984). Since, even at high angles, flow is reliably attached over at least three periphery ports as well as the center port, the probes can determine flow properties accurately over a wide angular range.

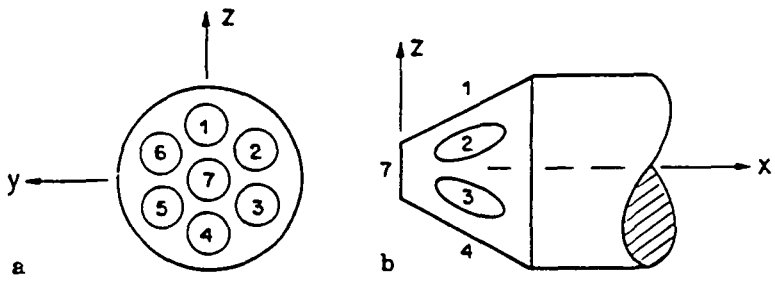

Figure 1a and b. Seven-Hole Probes: a) Front View Showing Port Numbering Convention and Principle Axes; b) Side View.

However, since the probes are so small in size, they are particularly sensitive to manufacturing variability. A comprehensive and statistically sound calibration process is therefore required prior to use. The calibration process relies on three independent pressure coefficients which depend only on probe-measured pressures at ports in the attached flow region. The coefficients are monotonic functions of the three independent flow variables (two flow angles and Mach number). For completeness, this paper briefly summarizes the calibration process as described in Gerner et al. (1984), Everett et al. (1983), and Gallington (1980).

The purpose of this research was to compare the accuracies of calibrations done with reduced matrices of data to those done with complete matrices of data. Previous calibrations (Gerner, Durston, Gallington) used from 252 to 1512 data points with seven independent regressions to calibrate a single probe. However, until now, there has been no direct comparison of calibrations of the same probe

using different amounts of calibration data or different matrices of calibration data of the same size.

This paper describes a complete calibration of two seven-hole probes. It first provides a summary of the development of the algorithms required for probe calibration. These algorithms provide the theoretical background for the development of the probe calibration computer program. This program converts a set of physical pressure measurements into a probe calibration model for use with the NASA Lewis data acquisition system.

Following the theoretical discussion, this paper describes the calibration matrices used to calibrate the two probes at NASA Lewis. One probe was calibrated with a complete matrix (approx. 1512 total data points) and with a reduced matrix (approx. 252 total data points). A second probe was calibrated with two independent reduced matrices (approx. 252 total data points each). Tables present comparison of the accuracies achieved with the various data matrices on both probes. The paper also describes a minor angular region asymmetry problem encountered during the calibration process and presents three approaches for handling this type of asymmetry.

The paper summarizes the development of a set of computer subroutines intended for use with the NASA Lewis data acquisition system. The subroutines use the calibration models to generate predictions of various flow properties in near real-time from probe-measured pressures.

Calibration pressure measurement taken during a check-out process of the NASA Lewis CE12 free jet facility indicated repeatability problems for port 7 at high subsonic Mach numbers within a small angular range. This paper describes the repeatability problem and provides signal frequency spectra which indicate that aliasing is the probable cause of the encountered problems.

2. Seven-Hole Probe Principles Summary

The ultimate objective of seven-hole probe design and calibration is to traverse the simple instrument through an unknown steady flow and extract all flow data obtainable from pressures. This flow data typically includes two flow angles and local total and dynamic pressures. Static pressure and Mach number then result from the compressible flow equations. The activities consisted of: (1) developing a set of algorithms and a corresponding probe calibration computer program to convert a set of physical measurements into a calibration model for use with the NASA Lewis Data Acquisition System; (2) taking a set of calibration data; (3) using the calibration program to compute the calibration model and to estimate expected errors; and (4) developing a set of subroutines which, when combined with the NASA Lewis Data Acquisition System, produce the desired flow data in near real-time from the raw probe-measured pressures. This section describes the techniques of each of these four activities and the experience of applying them at NASA Lewis Research Center.

2.1 Probe Calibration Algorithms and Computer Program

Preparation for the calibration process consists of three steps: (1) defining flow angle reference systems, (2) defining a complete set of independent pressure coefficients, and (3) defining calibration test matrices. Figure 2 defines three reference systems: conventional, polar, and tangent. Figure 3 defines seven symmetric pressure port angular region or sector boundaries. The polar reference system is most practical for the high flow angles (i.e., sectors 1 through 6). The tangential reference system is most practical for treatment of low flow angles (i.e., Sector 7). The complete systematic development of the relations in both reference systems is in Gallington (1980); a short summary follows.

Because the seven-hole probe naturally measures flow angles in three planes (one through each pair of diametrically opposed ports) instead of in two planes (as required by the α_T and β_T definitions and naturally achieved by a five-hole probe), the algorithm must combine the pressures in a sensible way to define two coefficients: one which varies strongly with α_T and the other with β_T.

As shown in Equation 1, the coefficient for determining α_T weighs the pressure difference between ports 1 and 4 at twice the pressure difference between ports 3 and 6 and twice the pressure difference between ports 5 and 2. The fact that the

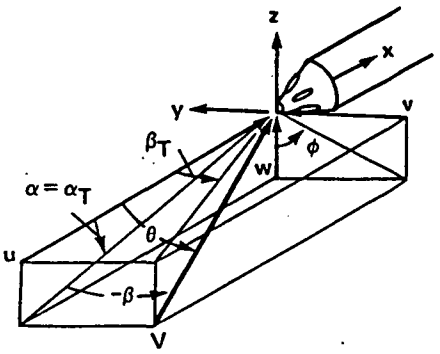

CONVENTIONAL	POLAR	TANGENT
$u = V \cos\alpha \cos\beta$	$u = V \cos\theta$	$\alpha_T = \arctan \frac{w}{u}$
$v = -V \sin\beta$	$v = V \sin\theta \sin\phi$	$\beta_T = \arctan \frac{v}{u}$
$w = V \sin\alpha \cos\beta$	$w = V \sin\theta \cos\phi$	

Figure 2. Reference System Definition from Gerner et al. (1984)

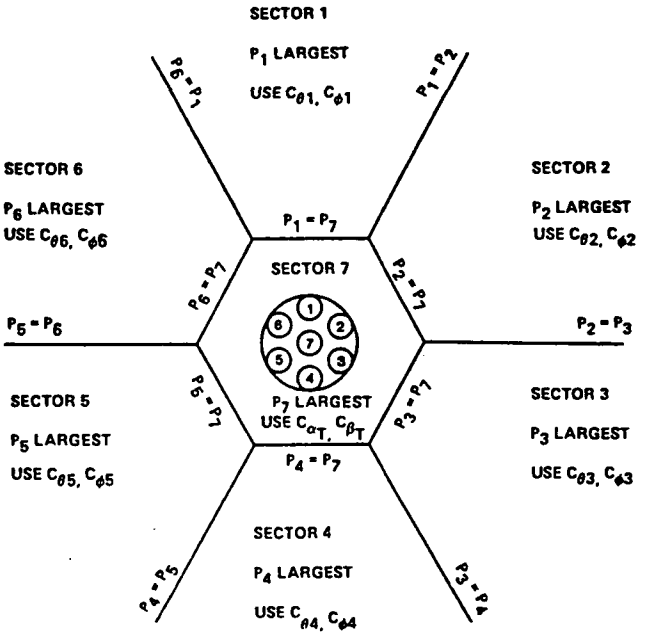

Figure 3. Angular Region Definitions from Gerner et al. (1984)

pressure difference between ports 1 and 4 is twice as sensitive to changes in α_T as is the pressure difference between ports 3 and 6 or the pressure difference between ports 5 and 2 requires these relative weights. Then the algorithm adds the three components and multiplies the total by an arbitrary 2/3. For determining β_T, the resulting algorithm must weigh the pressure difference between ports 2 and 5 and ports 3 and 6 equally. Further, the pressure difference between ports 2 and 5 and between ports 3 and 6 is $\frac{\sqrt{3}}{2}$ times as sensitive to changes in β_T as the pressure difference between ports 1 and 6 is to changes in α_T. Again, add all three components and multiply by the arbitrary 2/3. The pressure difference between ports 1 and 6 is insensitive to β_T and does not appear in Equation 2.

The complete set of independent pressure coefficients resolved into the tangential reference system, α_T-β_T, includes:

$$C_{\alpha T} = \frac{2}{3}\left(C_{\alpha a} + \frac{1}{2}C_{\alpha b} - \frac{1}{2}C_{\alpha c}\right) \quad (1)$$

$$C_{\beta T} = \frac{2}{3}\left(\frac{\sqrt{3}}{2}C_{\alpha a} + \frac{\sqrt{3}}{2}C_{\alpha b}\right) \quad (2)$$

and $$C_{M7} = (P_7 - \overline{P}_{1\text{-}6}) / P_7 \quad (3)$$

where $$C_{\alpha a} = (P_4 - P_1)/(P_7 - \overline{P}_{1\text{-}6}) \quad (4)$$

$$C_{\alpha b} = (P_3 - P_6)/(P_7 - \overline{P}_{1\text{-}6}) \quad (5)$$

$$C_{\alpha c} = (P_2 - P_5)/(P_7 - \overline{P}_{1\text{-}6}) \quad (6)$$

Gallington (1980) shows that the sensitivity of $C_{\alpha T}$ to α_T and the sensitivity of $C_{\beta T}$ to β_T are equal to about 0.07 per degree and that $C_{\alpha T}$ is nearly independent of β_T and $C_{\beta T}$ is nearly independent of α_T. Everett et al (1983) found sensitivities of about 0.075 per degree at low Mach number increasing to 0.08 per degree at a Mach number of 0.88. All previous work found the sensitivity of $C_{\alpha T}$ to α_T to be equal to the sensitivity of $C_{\beta T}$ to β_T thus supporting the symmetry of Equations 1 and 2.

The standard polar reference system was selected for the treatment of high flow angles (i.e., Sectors 1 through 6). The reference angles in this system are the pitch angle, θ, and the roll angle, ϕ. The complete set of pressure coefficients in this reference system includes:

$$C_{\theta n} = \{ (P_n - P_7)/[P_n - (P_{n-1} + P_{n+1})/2] \} \quad (7)$$

$$C_{\phi n} = \{ (P_{n-1} - P_{n+1})/[P_n - (P_{n-1} + P_{n+1})/2] \} \quad (8)$$

$$C_{Mn} = [P_n - (P_{n-1} + P_{n+1})/2]/P_n \quad (9)$$

where n represents the outer port numbers (n = 1, ..., 6). When n = 1, replace n-1 with 6, and when n = 6, replace n+1 with 1.

Unlike the local flow angles, the local total and dynamic pressures, which have dimensions, cannot be calculated directly. These pressures are extracted from two

types of additional dependent coefficients. These new dependent coefficients are determined explicitly from polynomial expressions which are functions of the full set of independent pressure coefficients. For low flow angles (i.e., Sector 7), the new dependent coefficients are:

$$C_O = (P_7 - P_{OL})/(P_7 - \overline{P}_{1\text{-}6}) \quad (10)$$

$$C_q = (P_7 - \overline{P}_{1\text{-}6})/(P_{OL} - P_{\infty L}) \quad (11)$$

For high flow angles (i.e., Sectors 1 through 6), the new dependent coefficients are:

$$C_{On} = (P_n - P_{OL})/[P_n - (P_{n-1} + P_{n+1})/2] \quad (12)$$

$$C_{qn} = [P_n - (P_{n-1} + P_{n+1})/2]/(P_{OL} - P_{\infty L}) \quad (13)$$

Each of these dependent coefficients contains both probe-measured pressures and desired pressure outputs. Knowing these dependent coefficients and the probe-measured pressures permits direct calculation of P_{OL} and $P_{\infty L}$. The calibration process uses a third-order polynomial expansion in three independent variables ($C_{\alpha T}$, $C_{\beta T}$, C_{M7} in the inner sector and C_θ, C_q, C_{Mn} in the outer sectors). Past experiments (Everett 1983) with the calibration of seven-hole probes in compressible flow show that this expansion adequately represents the parameter space. The expansion requires the twenty calibration constants (K_{ji}) appearing in Equation 14.

$$\begin{aligned} A_i = {} & K_{1i} + K_{2i}C_\theta + K_{3i}C_\phi + K_{4i}C_M + K_{5i}C_\theta^2 + K_{6i}C_\phi^2 + K_{7i}C_M^2 \\ & + K_{8i}C_\theta C_\phi + K_{9i}C_\theta C_M + K_{10i}C_\phi C_M + K_{11i}C_\theta^3 + K_{12i}C_\phi^3 \\ & + K_{13i}C_M^3 + K_{14i}C_\theta^2 C_\phi + K_{15i}C_\theta^2 C_M + K_{16i}C_\theta C_\phi^2 + K_{17i}C_\theta C_M^2 \\ & + K_{18i}C_\phi^2 C_M + K_{19i}C_\phi C_M^2 + K_{20i}C_\theta C_\phi C_M \end{aligned} \quad (14)$$

C_θ, C_ϕ, and C_M are the three independent pressure coefficients, K_{ji} are the calibration constants, and A_i is one of four flow properties (α_T or θ, β_T or ϕ, C_O or C_{On}, C_q or C_{qn}). In matrix notation, Equation 14 has the form

$$(A) = [C](K) \quad (15)$$

The Probe Calibration Computer Program accepts input files of experimental data from statistically adequate test matrices and produces a complete set of calibration constants for a particular probe. Figure 4 presents a flow chart of the program architecture. The program first reads and validates all test data from

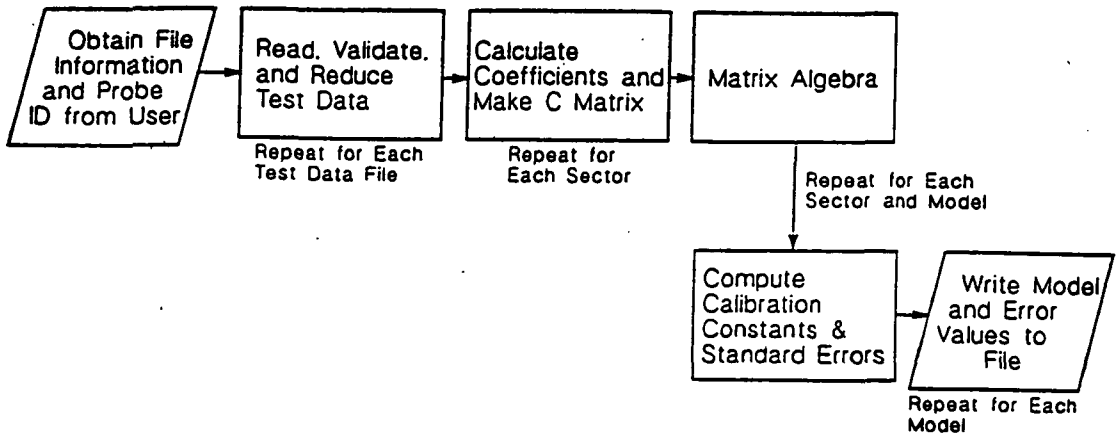

Figure 4. Probe Calibration Computer Program Flow Chart

files specified by the user. The program allocates each of the valid data points to the appropriate sector by locating the port with the largest measured pressure. The program then uses Equations 1 through 13 to compute the pressure coefficients for each test data point. The program uses matrix algebra to solve Equation 15 for the best (minimum variance) set of calibration constants. Equation 16 illustrates the required matrix algebra.

$$(K) = ([C]^T [C])^{-1} [C]^T (A) \tag{16}$$

Box (1978) derives Equation 16 and shows that it produces a set of constants (K) that minimizes the sum of the squares of differences between the measured values and the model. The program also provides the standard errors of the computed calibration models as calculated with Equation 17.

$$\sigma = \sqrt{\frac{(A_{ACTUAL} - A_{PREDICTED})^2}{N-M}}, \quad M = 20 \tag{17}$$

where σ is the standard error, A is a flow property, N is the number of data points, and M is the number of calibration constants.

2.2 Calibration Data Sets

Two types of calibration matrices are used during the calibration process: complete matrices and reduced matrices. The complete matrices populate the required parameter space with a uniform density of points. The reduced calibration matrices are constructed using the Latin Square technique. This technique provides a convenient method of obtaining homogeneous samples for large three-dimensional data sets. Gerner (1981) describes the use of Latin Squares to generate uniform density reduced data sets. Box et al (1978) describe a family of Latin Square designs and specifically describe the 6 x 6 (36 point) design used in this research. Figure 5 is one of many reduced test matrices. (Two of these matrices were generated for each sector of Probe 2.)

A complete matrix results from testing all six Mach numbers at each pair of angular values and has 6 times the 36 points in the reduced test matrix. Mach number spacing is closer near the high Mach number end because the independent pressure coefficients are more sensitive to Mach number there. The spacing is nearly even in the compressible flow function.

$$\frac{p_o - p_\infty}{p_o} = f\{M\} \tag{18}$$

In practice, it is not necessary to measure at exactly the point in the matrix. Missing a point by up to 20% of the difference between adjacent points has insignificant effect (Taguchi 1987).

Each polynomial (represented by Equation 14) requires 20 calibration constants. The 36 data points in a reduced matrix result in 16 degrees of freedom which is adequate to calculate the calibration constants and estimate the regression accuracy.

Angle of Roll, ϕ

Angle of Pitch, θ	155	165	175	185	195	205
30	M= 0.20	0.40	0.53	0.63	0.72	0.80
36	0.40	0.20	0.80	0.72	0.53	0.63
42	0.53	0.80	0.40	0.20	0.63	0.72
48	0.63	0.53	0.72	0.40	0.80	0.20
54	0.72	0.63	0.20	0.80	0.40	0.53
60	0.80	0.72	0.63	0.53	0.20	0.40

Figure 5. Reduced Calibration Matrix for Typical Outer Section 1.

2.3 Results of the Calibration Program Applied to Selected Data Sets

This section compares two different calibrations on each of the two probes. On Probe 1, a calibration for one sector using a complete matrix is compared with one using a reduced matrix. On Probe 2, the comparison is between two different reduced matrices. Repeatability errors discussed in Section 3 may affect all results in this section.

Figure 5 shows the a typical reduced matrix for Sector 1 of Probe 1. The complete matrix is the same except that all six values of Mach number occur at each pitch and roll angle. Note that the complete matrix has six times the number of data points as the reduced matrix. Table 1 presents standard error results for the complete matrix for Probe 1. These results are generated using Equation 17. The sectors contain an average of 212 data points. Standard error results are relatively constant through the outer sectors (i.e., sectors 1 though 6) and are significantly lower in the inner sector (i.e., Sector 7). These results are comparable with previous experiments (Gerner 1984). The results also show that the standard error for roll angle ($\sigma\ \theta$) in Sectors 1 and 4 is more than twice as large as in other outer sectors.

Table 2 compares the standard errors for the complete and reduced matrices for Sector 1 of Probe 1. Again, the standard errors are calculated using Equation 17. The standard errors calculated for the complete and reduced matrices are similar with the exception of $\sigma\ \theta$ and $\sigma\ \phi$. The values of $\sigma\ \theta$ and $\sigma\ \phi$ for the reduced matrix are 25% and 71% greater, respectively, than the complete matrix values. Table 2 also presents standard error values for the reduced matrix model applied to the complete data set. This comparison shows that the difference between the complete matrix and the model based on the reduced matrix is about 2.5 times the difference between the reduced matrix and the model based on the reduced matrix.

Table 1. Probe 1 Standard Error Results for the Complete Matrix

	Sector 1	Sector 2	Sector 3	Sector 4	Sector 5	Sector 6	Sector 7
$\sigma\ \theta(^\circ)$	0.590	0.802	0.703	0.765	0.673	0.691	0.153
$\sigma\ \phi(^\circ)$	0.720	0.387	0.327	0.953	0.571	0.362	0.191
σ M	0.011	0.013	0.013	0.011	0.013	0.014	0.006
$\sigma\ C_{o_n}$	0.007	0.010	0.009	0.010	0.009	0.008	0.008
$\sigma\ C_{q_n}$	0.025	0.031	0.033	0.031	0.031	0.030	0.007
Number of data points used in standard error calculation	236	189	186	275	185	193	221

Table 2. Comparison of Probe 1 Sector 1 Standard Error Results for the Complete Matrix and a Reduced Matrix

	Model Generated from Complete Matrix	Model Generated from a Reduced Matrix	
		Applied to Complete Matrix	Applied to Reduced Matrix
$\sigma\ \theta(^\circ)$	0.590	2.495	0.733
$\sigma\ \phi(^\circ)$	0.720	1.770	1.232
σ M	0.011	0.033	0.011
$\sigma\ C_{o_n}$	0.007	0.030	0.005
$\sigma\ C_{q_n}$	0.025	0.099	0.023
Number of data points used in standard error calculation	236	236	36

Tables 3 and 4 present estimates of the standard errors from two reduced matrices for Probe 2. These estimates were made in two ways. The first way estimates the accuracy of the curve fit to the data set used for calibration. Tables 3 and 4 show such standard errors for both reduced matrices. The standard errors are comparable indicating that the models fit their corresponding data sets equivalently.

Table 3. Probe 2 Standard Error Results for Reduced Matrix 1

	Sector 1	Sector 2	Sector 3	Sector 4	Sector 5	Sector 6	Sector 7
$\sigma\ \theta(^\circ)$	0.994	1.292	1.386	1.024	1.320	0.988	0.324
$\sigma\ \phi(^\circ)$	1.331	1.018	0.836	3.946	1.358	3.047	0.791
σ M	0.015	0.016	0.015	0.013	0.011	0.011	0.007
$\sigma\ C_{o_n}$	0.009	0.011	0.011	0.012	0.009	0.009	0.011
$\sigma\ C_{q_n}$	0.039	0.051	0.047	0.027	0.027	0.027	0.009
Number of data points used in standard error calculation	36	34	36	37	37	46	41

Table 4. Probe 2 Standard Error Results for Reduced Matrix 2

	Sector 1	Sector 2	Sector 3	Sector 4	Sector 5	Sector 6	Sector 7
$\sigma\ \theta(^\circ)$	0.969	1.485	0.988	0.731	0.710	0.761	0.350
$\sigma\ \phi(^\circ)$	1.274	0.652	0.832	3.374	0.661	0.535	0.844
σ M	0.012	0.017	0.013	0.010	0.014	0.008	0.007
$\sigma\ C_{o_n}$	0.008	0.011	0.011	0.011	0.007	0.005	0.009
$\sigma\ C_{q_n}$	0.031	0.043	0.030	0.018	0.027	0.032	0.009
Number of data points used in standard error calculation	36	34	43	35	34	30	41

The second way estimates the accuracy that the calibration using one data set fits the other data set. Table 5 shows how well the Reduced Matrix 1 model fits the

Reduced Matrix 2 data. The standard error in the roll angle measurement in Sectors 4 and 6 are significantly higher than the others. These anomalously high standard errors may result from the repeatability problems discussed in Section 3 of this report. The standard errors associated with how well the calibration predicts an independent data set are two to three times larger than the standard error associated with fitting the curves to the calibration matrix.

Table 5. Probe 2 Standard Error Results for Reduced Matrix 2 Data Using Reduced Matrix 1 Model

	Sector 1	Sector 2	Sector 3	Sector 4	Sector 5	Sector 6	Sector 7
$\sigma\ \theta(^\cdot)$	3.466	3.036	1.728	2.205	2.298	3.964	0.668
$\sigma\ \phi(^\cdot)$	3.256	1.776	1.825	6.638	2.315	9.004	1.404
σ M	0.047	0.049	0.018	0.021	0.037	0.030	0.011
$\sigma\ C_{O_n}$	0.027	0.024	0.026	0.027	0.013	0.021	0.021
$\sigma\ C_{q_n}$	0.162	0.096	0.056	0.077	0.084	0.114	0.019
Number of data points in sector	36	34	43	35	34	30	41

As in previous calibrations, (Gallington [1980], Gerner [1984], Gerner [1981], Everett [1983]) the original geometrical definitions of the sector boundaries did not match the sector boundaries defined by the pressures. There are three equally acceptable resolutions. The first approach uses the data points originally assigned to a sector to do the calibration even though some of the points defining the calibration would be outside the space in which the calibration was used. This approach was taken in the previous NASA work (Everett 1983) and was nominally successful.

A second approach includes an initial screening experiment to find the sector boundaries and then adjusts the calibration data sets to fit approximately uniformly inside these boundaries. Although the most robust, this second approach adds another calibration tunnel entry to the procedure, negating some of the time savings resulting from using the reduced data set in the first place.

The third approach, and the one used in this research, uses all the calibration data that falls into a sector based on the pressure definitions. This approach may put more points in some sectors than others and thus destroy some of the

symmetry of the Latin Squares matrix design. On the other hand, it avoids the obvious extrapolation of the first approach and contains a certain self-correcting feature. If the sector boundary is distorted to a larger than expected size, the additional points will help fit the calibration curves over this larger range. A sector may become so sparse in calibration data that the calculation of the 20 constants in the calibration curves becomes fragile. There is an easy way to check for this problem. If the number of calibration points minus the number of calculated constants (in statistics, the degrees of freedom) becomes too small, an inaccurate calibration is likely. In this study, there are always 20 calculation constants. The last row of Tables 3 and 4 show that, by this measure, there was adequate data in each sector to make a good estimate.

2.4 Data Acquisition System Flow Property Subroutines

The Flow Property Subroutines use the calibration models computed by the probe calibration computer program along with the seven acquired port pressures to predict two flow angles, and the total and dynamic pressures.

Figure 6 presents a functional flow chart of the subroutines. The first subroutine called by the Data Acquisition System reads in the calibration constants for the specified probe. As pressure readings are taken, the Data Acquisition System calls another subroutine which computes the pressure coefficients and performs the matrix algebra shown in Equation 15 to output the predicted flow properties in near real-time.

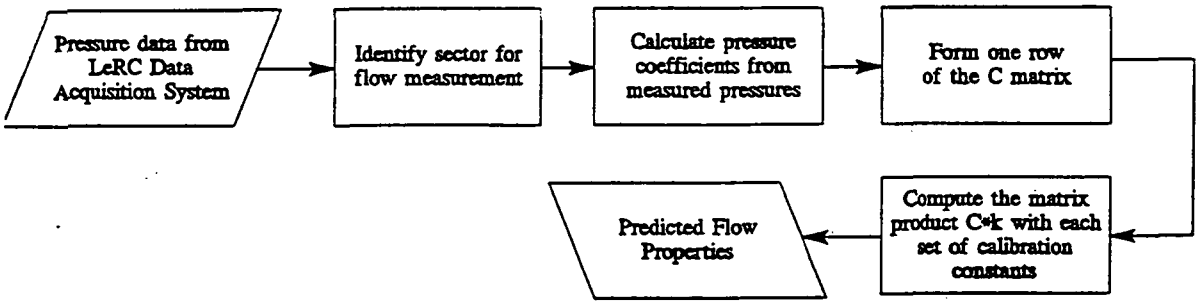

Figure 6. Functional Flow Chart of Flow Property Subroutines

3. Aliasing and Repeatability Problems

Over a narrow range of angles and Mach numbers in one of the NASA Lewis facilities (CE12) used for calibration of Probe 2, some probe measured pressures were not adequately repeatable. This problem either did not occur or was not noticed in the other NASA Lewis facility (W8) used for calibration of Probe 1. The Lewis Research Center check out procedure indicated that the measured pressures (after the averaging process) are not stationary, but vary significantly with time. The source of this variation remains unknown.

During seven-hole probe calibration, only the quasi-stationary value of pressure measurements (steady-state values) are desired and thus calibration equipment should seek to minimize excursions as they result in potential error sources. There are two types of errors to avoid during the seven-hole probe calibration process: errors due to unwanted fluctuations that are the result of the process or equipment and errors due to insufficient aperture time. Figure 7 illustrates the regions of error as a function of the frequency of the error signal.

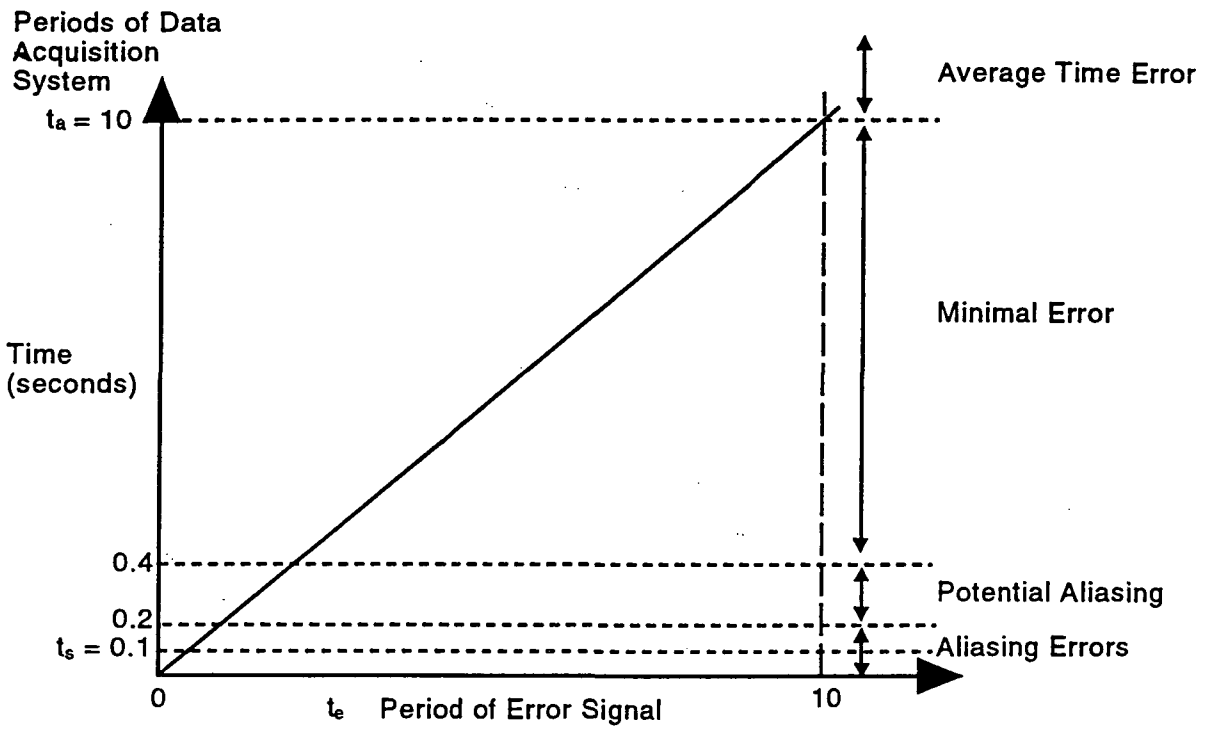

Figure 7. Potential Error Sources in Data Acquisition

Both NASA Lewis facilities, W8 and CE12, use a two-step data acquisition system consisting of an Electronically Scanned Pressure (ESP) module followed by the Escort System. The system has no anti-aliasing filters. The combined system (ESP and Escort) uses 100 samples over a span of 10 seconds to determine the steady state pressure. The ESP module samples the pressure for one second at a rate of 10 samples per second (10 Hz) and averages these 10 samples to produce one value. Each time a data point is requested, the Escort System collects 10 values from the ESP. Each of these values is, in turn, the average of 10 samples. The Escort System then averages these 10 values to produce a steady state pressure measurement.

The Lewis Research Center data acquisition system measures the pressure in the chamber at 0.1 second intervals (i.e., $f_s = 10$ Hertz). The Nyquist sampling theorem states that a signal that is ideally band-limited can be reconstructed if the sampling rate is at least twice the highest (or cutoff) frequency (Doebelin 1983). Thus, when $f_s \geq 2\ f_c$, frequency distortion (aliasing) does not occur. Since practical signals are not ideally band-limited, the relationship $f_s \geq 4\ f_c$, is used in practice, as illustrated in Figure 7.

The averaging time is defined as the total sampling time. The Lewis Research Center data acquisition system takes 100 pressure measurements in 10 seconds and hence, the aperture time t_A is 10 seconds. If the period of the error signal is greater than 10 seconds, then a bias is introduced in the measured pressure.

Figure 8 shows sketches of the frequency spectra indicating high frequency components of about 20 and 40 Hertz in the measured pressure signal. The existence of significant noise energy above one-half the sampling frequency will cause aliasing. Indeed, because most of the energy is concentrated at about twice and four-times the sampling frequency the aliasing error will appear in the output as a DC offset. This is consistent with the slowly wandering data coming out of the data acquisition system. This problem was observed only in the Sector 6 data over a narrow range of angles and Mach numbers. Frequency spectra suggest it did occur in other ranges, but was not noticed. This is a possible explanation why the standard error reported in this research are slightly higher than those reported by Everett (1983) and Gerner
(1984).

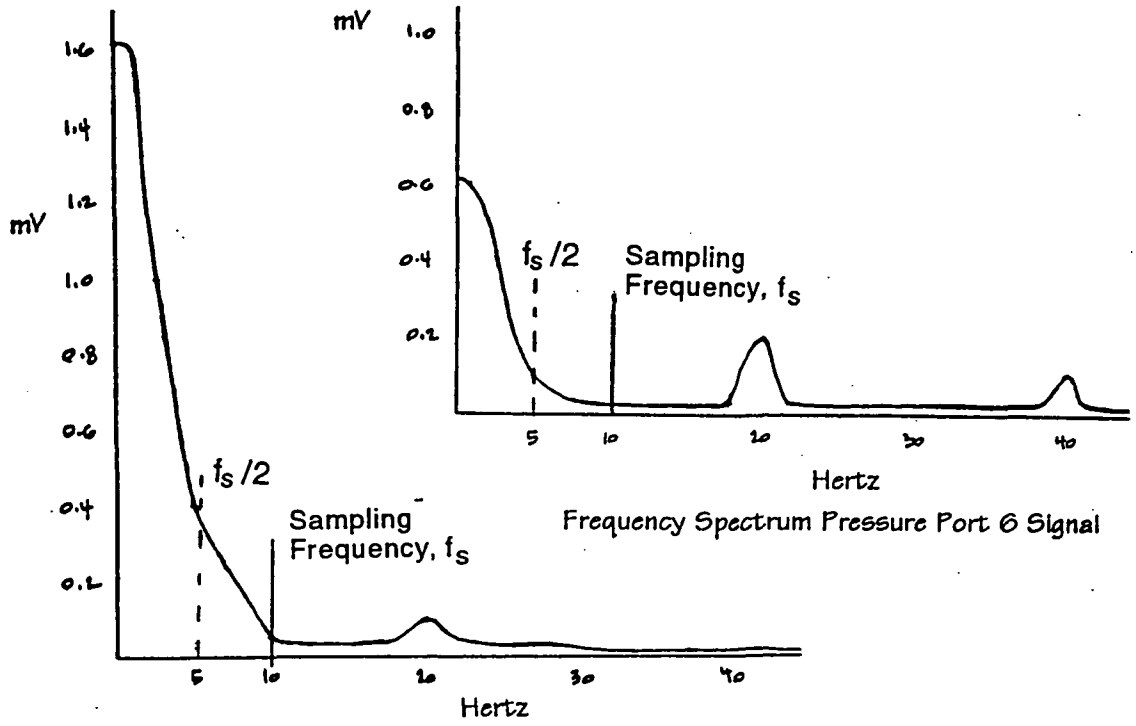

Figure 8. High Frequency Components of 20 and 40 Hz

4. Conclusions

The seven-hole probe calibration indicated about the same average useful angular range and accuracy of regression curve fit as previous calibrations of similar probes. However, the accuracy with which a model predicted data in a matrix other than the one used to define the model was about 2.5 times worse (i.e. the standard error was 2.5 times larger) than the standard error of the regression. At high angles expected standard errors in measuring unknown flow fields are about three degrees in angle and about 0.03 in Mach number. At low angles, expected standard errors were about one degree in angle and about 0.01 in Mach number. This level of calibration accuracy was achieved with reduced test matrices containing seven sets of about 36 points each. Full test matrices containing seven sets of about 252 points each improve accuracy by about a factor of 2.5. The data reduction program computes reduced data from probe pressures.

Errors are not necessarily uniformly distributed. Errors were apparent in one facility over a narrow angular range at the higher Mach numbers. In this range, there is a lack of repeatability apparently due to aliasing. Interaction of 20 and 40 Hertz noise components with the 10 Hertz sampling frequency produced aliasing which can produce apparent low frequency signals which the subsequent averaging process cannot remove. These frequencies are typical of mechanical vibration and are subharmonics of 60 Hertz power.

References

Gerner, A.A., C.L. Maurer, R.W. Gallington, "Non-nulling Seven-Hole Probes for High Angle Flow Measurement", Experiments in Fluids 2, pp 95-108, 1984.

Doebelin, Ernest O., Measurement Systems Application and Design, McGraw-Hill Book Company, pp 445-446, 1983.

Everett, K.N., A.A. Gerner, and D.A. Durston, "Seven-Hole Cone Probes for High Angle Flow Measurement: Theory and Calibration", AIAA Journal, Vol 21, No.7, (1983)

Gallington, R.W., "Measurement of Very Large Flow Angles with Non-Nulling Seven-Hole Probes," Aeronautics Digest--Spring/Summer 1980, USAFA-TR-80-17, USAF Academy 1980.

Box, G.E.P., W.G. Hunter, and J.S. Hunter, Statistics for Experiments, John Wiley & Sons, pp 261-263, 1978.

Gerner, A.A., and C.L. Maurer, "Calibration of Seven-Hole Probes Suitable for High Angle in Subsonic Compressible Flows," Aeronautics Digest--Fall/Winter 1980, USAF-TR-81-4, USAF Academy, 1981.

Taguchi, G., System of Experimental Design, American Supplier Institutes, Inc., Vol. 2, p 613, 1987.

Box, G.E.P., W.G. Hunter, and J.S. Hunter, Statistics for Experiments, John Wiley & Sons, pp 501-502, 1978.

REPORT DOCUMENTATION PAGE

Form Approved
OMB No. 0704-0188

1. AGENCY USE ONLY (*Leave blank*)	2. REPORT DATE	3. REPORT TYPE AND DATES COVERED
	September 1995	Technical Memorandum

4. TITLE AND SUBTITLE
Rapid Calibration of Seven-Hole Probes

5. FUNDING NUMBERS
WU-505-68-30

6. AUTHOR(S)
A.L. Ericksen, R.W. Gallington, B.M. Rao, and W.S. Barankiewicz

7. PERFORMING ORGANIZATION NAME(S) AND ADDRESS(ES)
National Aeronautics and Space Administration
Lewis Research Center
Cleveland, Ohio 44135-3191

8. PERFORMING ORGANIZATION REPORT NUMBER
E-9868

9. SPONSORING/MONITORING AGENCY NAME(S) AND ADDRESS(ES)
National Aeronautics and Space Administration
Washington, D.C. 20546-0001

10. SPONSORING/MONITORING AGENCY REPORT NUMBER
NASA TM-107040

11. SUPPLEMENTARY NOTES
A.L. Ericksen, R.W. Gallington, and B.M. Rao Science Applications International Corporation, 445 Market Place One, 2001 Western Avenue, Seattle, Washington 98121-2114 (work funded by NASA Contract NAS3-27008); W.S. Barankiewicz, NASA Lewis Research Center. Responsible person, W. S. Barankiewicz, organization code 2780, (216) 433-8706.

12a. DISTRIBUTION/AVAILABILITY STATEMENT
Unclassified - Unlimited
Subject Category 07

This publication is available from the NASA Center for Aerospace Information, (301) 621-0390.

12b. DISTRIBUTION CODE

13. ABSTRACT (*Maximum 200 words*)

This paper summarizes the major conclusions and some of the key supporting analyses resulting from the calibration and application of two small seven hole probes at NASA Lewis Research Center. These probes can produce reasonably accurate and rapid surveys of unknown steady flow fields which may include flow angles up to 70 degrees and Mach numbers up to 0.8. The probes were calibrated with both "complete" and "reduced" test matrices. Both types of test matrices produced similar results suggesting that the reduced matrices are adequate for most purposes. The average accuracy of the calibration was about the same as that achieved in previous seven hole probe calibrations. At the higher Mach numbers, the calibration was sensitive to the diameter of the free jet in the calibration facility. Over a narrow angular range at the higher Mach numbers, the system had serious repeatability problems. This lack of repeatability apparently results from aliasing of high frequency (20 and 40 Hertz) noise with the data acquisition system sampling frequency of 10 Hertz. Analyses show that these noise frequencies are probably not related to airflow dynamics in the connecting tubing.

14. SUBJECT TERMS	15. NUMBER OF PAGES
Wind tunnel instrumentation; Probes	22
	16. PRICE CODE: A03

17. SECURITY CLASSIFICATION OF REPORT	18. SECURITY CLASSIFICATION OF THIS PAGE	19. SECURITY CLASSIFICATION OF ABSTRACT	20. LIMITATION OF ABSTRACT
Unclassified	Unclassified	Unclassified	